Inorganic Chemistry

Article

pubs.acs.org/IC

Homometallic Cubane Clusters: Participation of Three-Coordinated Hydrogen in 60-Valence Electron Cubane Core

K. Yuvaraj,[†] Dipak Kumar Roy,[†] Bijan Mondal,[†] Babu Varghese,[‡] and Sundargopal Ghosh*,[†]

[†]Department of Chemistry, Indian Institute of Technology Madras, Chennai 600 036, India

[‡]Sophisticated Analytical Instruments Facility, Indian Institute of Technology Madras, Chennai 600 036, India

Supporting Information

ABSTRACT: This work describes the synthesis, structural characterizations, and electronic structures of a series of novel homometallic cubane clusters $[(Cp^*Ru)_2\{Ru(CO)_2\}_2BH(\mu_3\text{-}E)(\mu\text{-}H)B(\mu\text{-}H)_3M]$, (**2**, M = Cp*Ru, E = CO; **3**, M = $Ru(Cp^*Ru)_2(\mu\text{-}CO)_3(\mu\text{-}H)BH$), E = BH), $[(Cp^*Ru)_3(\mu_3\text{-}CO)(BH)_3(\mu_3\text{-}H)_3]$, **4**, and $[(Cp^*Ru)_2(\mu_3\text{-}CO)\{Ru(CO)_3\}_2(BH)_2(\mu\text{-}H)B]$, **5** (Cp* = η^5-C_5Me_5). These cubane clusters have been isolated from a thermally driven reaction of diruthenium analogue of pentaborane(9) $[(Cp^*RuH)_2B_3H_7]$, **1**, and $[Ru_3(CO)_{12}]$. Structural and spectroscopic studies revealed the existence of triply bridged hydrogen (μ_3-H) atoms that participate as a vertex in the cubane core formation for compounds **2**, **3**, and **4**. In addition, the crystal structure of these clusters clearly confirms the presence of an electron precise borane ligand (borylene fragment) which is triply bridged to the trimetallic units. Bonding of these novel complexes has been studied computationally by DFT methods, and the studies demonstrate that the cubane clusters **2** and **3** possess 60 cluster valence electrons (cves) with six metal−metal bonds. All the new compounds have been characterized in solution by mass spectrometry; IR; and ^1H, ^{11}B, and ^{13}C NMR studies, and the structural types were unequivocally established by crystallographic analysis of compounds **2**−**5**.

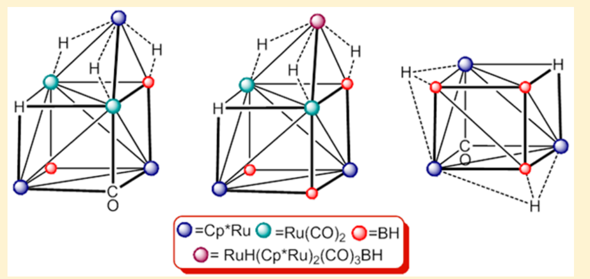

■ INTRODUCTION

Cubic structures had been observed in inorganic chemistry before the synthesis of cubane (C_8H_8) in 1964 by Eaton and Cole.[1] Metal complexes with cubane core have inspired significant interest due to their potential use as models for various industrial and biological catalytic processes.[2−4] The cube, aesthetically satisfying for its high symmetry, is well-characterized in elements in both the p-block and d-block and in combination of the two. The most common type of cubane structure is that in which two types of vertices are present, i.e., M_4E_4 (E = S, Se, Te, P, Sb, Bi, CO), a tetrahedral structural motif with four metal atoms and four main group elements.[5−8] While a large number of cubanes in which the E and M fragments are composed of either main group and transition metals or exclusively main group elements have been known for decades,[5−8] the search for clusters having boron in the cubane core have been met with little success.[9,10] Despite the remarkable growth in this field, advances have been slow, and only a handful of such clusters are reported (**I**−**IV**; Chart 1).[9,10]

Our research group has been interested in the synthesis of "hybrid" clusters that comprise metal and boron atoms in comparable numbers and display properties mutual to both the borane and metal cluster families.[11,12] Polynuclear metal carbonyl compounds have proven to be useful precursors for many cluster-growth reaction in metallaborane chemistry.[13] As a result, we have extended our studies to transition-metal carbonyl compounds in association with their versatility in metal cluster-growth reactions.[14,15]As a general methodology for the synthesis of higher-nuclearity metallaborane clusters, we have carried out the reaction of diruthenium analogue of pentaborane(9), *nido*-$[1,2(Cp^*RuH)_2B_3H_7]$, **1**, with $[Ru_3(CO)_{12}]$. In this Article, we present the synthesis, structural analysis, and electronic structure of a series of homometallic cubane clusters.

Chart 1. Known Homo- and Heterometallic Cubane Type Clusters Containing Boron as a Vertex (Cp = η^5-C_5H_5, Cp* = η^5-C_5Me_5)

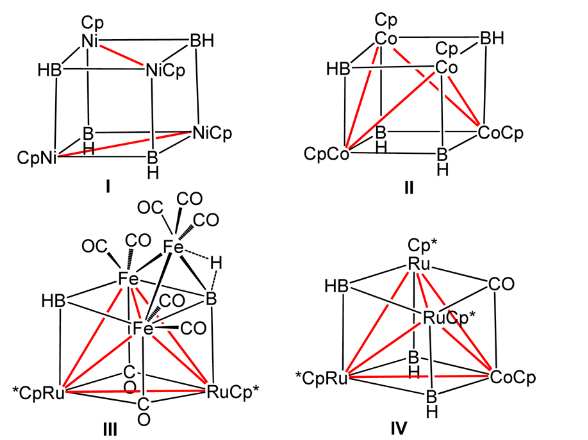

Received: June 9, 2015
Published: August 19, 2015

DOI: 10.1021/acs.inorgchem.5b01298
Inorg. Chem. 2015, 54, 8673−8678

Scheme 1. Synthesis of Homometallic Cubanes 2−5

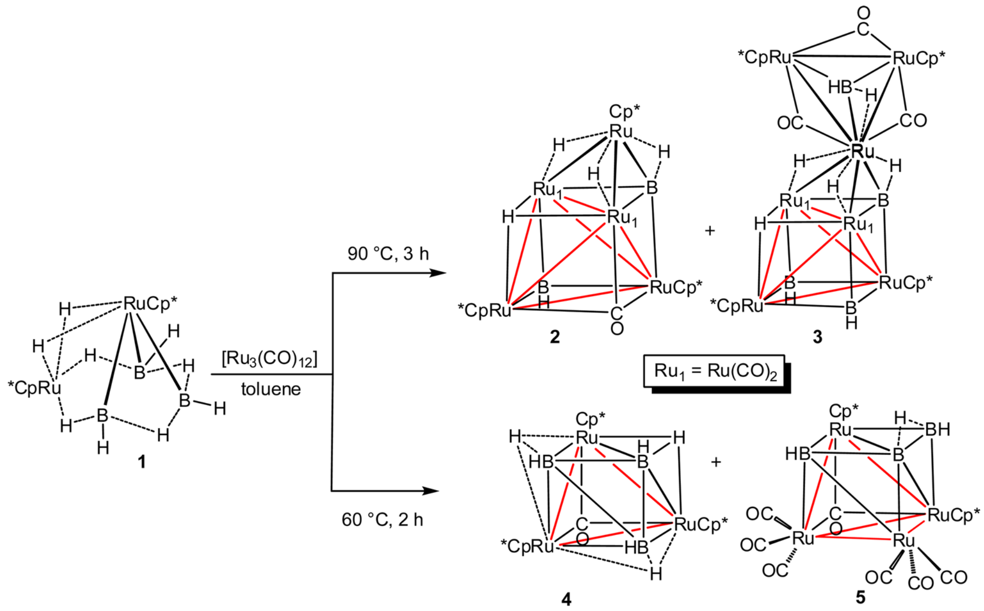

■ RESULTS AND DISCUSSION

Homometallic Cubane Clusters 2 and 3. As shown in Scheme 1, thermolysis of **1** with $[Ru_3(CO)_{12}]$ generated homometallic cubane type clusters, $[(Cp^*Ru)_2\{Ru(CO)_2\}_2BH(\mu_3\text{-E})(\mu_3\text{-H})B(\mu\text{-H})_3M]$, (**2**, M = Cp*Ru, E = CO; **3**, M = $RuH(Cp^*Ru)_2(CO)_3BH$), E = BH) in moderate yields. Compounds **2** and **3** were separated from the reaction mixtures by thin-layer chromatography as orange and brown solids, respectively. They have been characterized by spectroscopic techniques, elemental analysis, and single crystal X-ray diffraction study. The $^{11}B\{^1H\}$ NMR spectrum of **2** displayed two resonances with equal intensities; the peak at δ = 129.5 ppm was assigned to the borylene boron atom, and the most downfield resonance at δ = 141.7 ppm that implies a greater degree of boron−metal interaction was assigned to the boride boron atom (B1) (Figure 1a). In the case of compound **3** the ^{11}B NMR of **2** shows the presence of three peaks at δ = 151.7, 128.9, and 95.1 ppm. In a comparison of the ^{11}B NMR chemical shift values of **3** with **2** and other metallaboranes,[10a,11c,14a] the peak at 151.7 ppm has been assigned to the boride boron atom (B2) (Figure 1b). The ^1H NMR spectrum of **2** features three types of Cp* resonances that appeared at δ = 1.95, 1.78, and 1.64 ppm, indicative of two different Ru environments.

Besides the Cp* protons, the ^1H NMR shows one BH proton and three upfield signals at δ = −6.57, −10.0, and −16.41 ppm in 1:2:1 ratio. The $^{11}B\{^1H\}/^1H\{^{11}B\}$ HSQC experiment reveals the most downfield ^{11}B peak (141.7 ppm) associated with the proton at −6.57 ppm, whereas other two upfield protons did not couple with any boron unit. The ^1H NMR spectrum of **3** shows three types Cp* resonances in 1:2:1 ratio along with upfield chemical shifts at δ = −1.73, −11.14, −13.41, −15.72 ppm. Similarly, the $^{11}B\{^1H\}/^1H\{^{11}B\}$ HSQC experiment of compound **3** demonstrates that the most downfield ^{11}B peak (151.7 ppm) is coupled with the proton at −11.14 ppm, whereas the peak at −1.73 ppm is associated with the ^{11}B peak at 95.1 ppm.

Solid State X-ray Structures of 2 and 3. The crystal structures of **2** and **3**, shown in Figure 1a,b, clearly display the presence of the cubane core in which one of the vertices is occupied by a hydrogen atom. Significant disorder was observed involving the permutation of the BH and CO fragments in **2**; therefore, the structural parameters discussed herein are from one of the residues (see X-ray structure details and Supporting Information for further details of the disorder). The core geometry of them can be projected in two different ways. The easiest approach is to categorize them as a cubane core anchored to an *exo*-fragment. The cubane core in the case of **2** is composed of four rutheniums (Ru1, Ru2, Ru4, and Ru5), two borons (B1, B3), one CO, and one μ_3-hydrogen atom (H1) (Figure 1a). The intriguing feature of **3** is the presence of a triply bridged borylene unit as an *exo*-fragment (Figure S2). In a different view, both compounds **2** and **3** can be described as a Ru_4 tetrahedron, in which all the four triangular faces of **2** are capped by one CO ligand, two borons,

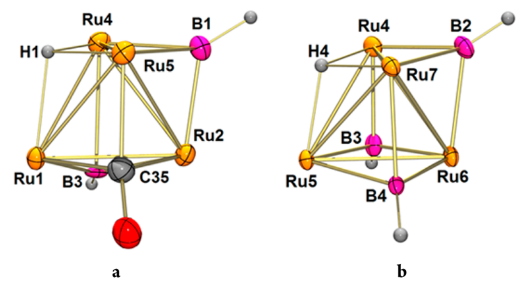

Figure 1. (a, b) Molecular structures and labeling diagrams of **2**, **3** (only core geometries are shown; Cp* and CO ligands on Ru atoms are not shown for clarity). Thermal ellipsoids are shown at the 20% probability level. Selected bond lengths [Å]: (a) **2** B1−Ru2 1.967(9), B1−Ru4 2.173(9), B1−Ru5 2.176(8), Ru1−C35 2.07(4), Ru1−B3 2.12(5), Ru1−Ru2 2.7282(8), Ru1−Ru4 2.7889(8), Ru1−Ru5 2.7948(9), Ru1−H1 1.93(6), Ru2−C35 2.15(4), Ru2−B3 2.19(5), Ru2−Ru5 2.7853(8), Ru4−B3 2.50(4), Ru4−Ru5 2.8478(8), Ru4−H1 1.82(6); (b) **3** B2−Ru6 1.972(6), B2−Ru4 2.180(6), B2−Ru7 2.184(6), B3−Ru5 2.057(7), B3−Ru6 2.117(7), B3−Ru4 2.190(6), B4−Ru5 2.065(7), B4−Ru6 2.118(7), B4−Ru7 2.195(6), Ru4−H4 1.83(5), Ru5−H4 1.77(5), Ru4−Ru5 2.7691(6), Ru4−Ru6 2.7767(6), Ru4−Ru7 2.8484(6), Ru5−Ru6 2.7448(7), Ru5−Ru7 2.7644(6), Ru7−H4 1.84(5).

DOI: 10.1021/acs.inorgchem.5b01298
Inorg. Chem. 2015, 54, 8673−8678

and one hydrogen. On the other hand, the triangular faces of **3** are capped by three boron atoms and one hydrogen. The average M−M−M angle, observed in both **2** (59.76°) and **3** (59.17°), are very close to the regular tetrahedron one (60°).

Thermolysis of *nido*-**1** with [$Ru_3(CO)_{12}$] yielded 60 cve **2** and **3**. The reaction pathway whereby these novel cubanes are formed is unknown; however, the isolation of [$(Cp^*Ru)_3(\mu_3\text{-}CO)(BH)_3(\mu_3\text{-}H)_3$], **4** (Figure 2a), and [$(Cp^*Ru)_2(\mu_3\text{-}CO)\{Ru(CO)_3\}_2(BH)_2(\mu\text{-}H)B$], **5** (Figure 2b), reveals a likely path for the formation of **2** and **3**. Having looked at the molecular structures of **2**−**5**, one can visualize the formation of **4** from *nido*-**1** replacing three hydrogens (3e) with one CO (2e) and one {Cp*Ru} (1e) fragment. Thus, the presence of extra metal fragments in **2** drives us to carry out reaction of *nido*-**1** with [$Ru_3(CO)_{12}$] under different reaction conditions. Cluster **5** contains 62 cves with five metal−metal bonds; thus, it is reasonable to assume that the 60 cve species **2** with six M−M bonds might have formed during the course of reaction. Although conversion of **5** to **2** was successful (Figures S15 and S16), all of our attempts to generate **5** from **4** failed.

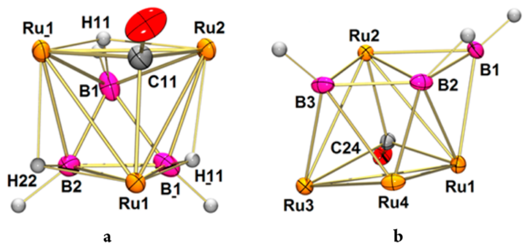

Figure 2. (a, b) Molecular structures and labeling diagrams of **4**, **5** (only core geometries are shown; Cp* and CO ligands on Ru atoms are not shown for clarity). Thermal ellipsoids are shown at the 20% probability level. Selected bond lengths [Å]: (a) **4** B1−B2 1.71(3), B1−B_1 1.80(5), B_1−Ru1 2.27(2), B1−Ru2 2.30(2), B1−H11 1.15(2), B2−Ru_1 2.34(3), B2−Ru1 2.34(3), B2−H22 1.15(2), Ru−1−Ru1 2.804(2), Ru1−Ru2 2.8128(16), Ru2−B_1 2.30(2), Ru2−Ru_1 2.8128(16), C11−Ru1 2.068(18); (b) **5** C24−Ru1 2.035(4), C24−Ru3 2.508(4), B1−B2 1.660(7), B1−Ru2 2.132(4), B1−Ru1 2.145(4), B2−B3 1.711(7), B2−Ru4 2.101(4), B2−Ru2 2.163(4), B2−Ru1 2.182(4), B3−Ru2 2.161(4), B3−Ru3 2.214(4), B3−Ru4 2.283(5), Ru1−Ru2 2.7288(4), Ru1−Ru3 2.8619(4), Ru1−Ru4 2.8667(4), Ru2−Ru3 2.7985(4), Ru3−Ru4 2.7796(5).

Electronic Spectra and Electrochemical Study. The cubane clusters reported here contain either three or four metal centers in the cubane core. Thus, to see the difference in the absorption pattern, the electronic spectra of compounds **2-5** in the visible region (in a CH_3CN solution) has been measured (Figure 3 and Figure S9). In essence, there are single absorption bands for **2** and **3** at 206, 209 nm with indications of several weaker bands at lower energy. The pattern of these spectra is very similar to that of the homometallic cubane clusters, [$(CpNi)_4B_4H_4$][9] and [$(Cp^*Mo)_4B_4H_4(\mu_4\text{-}BH)_3$].[9c] As shown in Table 1, the higher intensity bands at 206 and 209 nm have been blue-shifted by *ca.* 80 nm on going from [$(CpNi)_4B_4H_4$] to **2** and **3**. This may be due to the presence of the {$\eta^5\text{-}C_5Me_5$} ligand, which generally produces a stronger ligand field than the {$\eta^5\text{-}C_5H_5$} ligand.[16] In order to get some insight into the redox properties of the cubanes, we performed electrochemical measurements on **2**−**5**. The cyclic voltammograms, shown in Figures S5 and S6, underwent various irreversible and quasireversible redox processes for these cubane clusters.

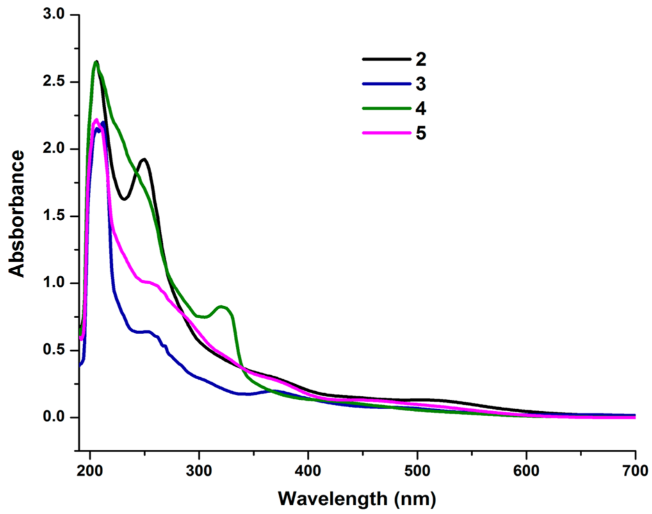

Figure 3. UV−vis spectra of compounds **2**−**5** in CH_3CN (10^{-3} M).

Table 1. UV−Vis Spectra of 2−5 and Analogous Cubane Clusters

compd	λ_{max}, nm	ref
[$(CpNi)_4B_4H_4$]	543, 423, 335, 284	9a
[$(CpNi)_4B_5H_5$]	548, 365, 302, 257	9a
[$(Cp^*Cr(\mu\text{-}O)]_4$	596	17
[$(MeCp)_4Mo_4S_4$]	520	18
[$(Cp^*Mo)_4B_4H_4(\mu_4\text{-}BH)_3$]	440, 367, 315, 239	9c
2	513, 368, 248, 206	this work
3	499, 370, 253, 209	this work
4	429, 318, 204	this work
5	481, 372, 258, 204	this work

Quantum-Chemical Calculation. The ^{11}B and ^1H NMR chemical shifts were calculated using B3LYP functional (see Computational Details)[22] and compared with the experimental values of clusters **2**−**5** (Tables S1 and S2). Good agreement has been observed both for ^1H and ^{11}B chemical shift values. The theoretical study allowed us to distinguish not only the difference in connectivity of the hydrogen (μ_2 or μ_3) but also the different environments of the boron atoms. The schematic representation of the μ_3-H connectivity in **2**, as obtained from MO analysis, is shown in Figure 4. The natural bond orbital (NBO) analysis[23] calculated for **2** (Table S3) demonstrates that the triply bridged hydrogen (natural charge −0.24) is more hydridic compared to the doubly bridged Ru−H−B (−0.12) and Ru−H−Ru (−0.21). Therefore, the shielded μ_3-H atoms for **2** and **3** appear at the upfield region in ^1H NMR. The Wiberg bond indices[23] (WBIs) of Ru−H coupling *ca.* 0.25 further establish the μ_3-H connectivity (Table S4).

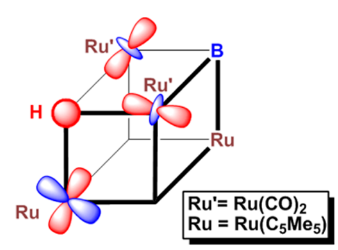

Figure 4. Molecular orbital scheme showing μ_3-H connectivity for **2** and **3**.

DOI: 10.1021/acs.inorgchem.5b01298
Inorg. Chem. 2015, 54, 8673−8678

The essential difference between the geometries of **2** and **3** is the moiety attached to the *exo*-Ru center (Figures S1 and S2). For **2** it is a Cp* ligand, whereas **3** possesses $\{(Cp^*Ru)_2(CO)_3BH(\mu\text{-}H)\}$. To validate if clusters **2** and **3** are isoelectronic, the MO and NBO calculations were undertaken. The WBI values signify that Ru3 in the exofragment of **3** is bonded with Ru1 and Ru2. In addition, B1 is bonded to Ru3 through a 3c−2e bond (Figure S8). Therefore, the total valence electron count around Ru3 amounts to 13, which is the same as that for Cp*Ru. As a result, the $\{(Cp^*Ru)_2(CO)_3BH(\mu\text{-}H)\}$ moiety contributes 5 electrons to the Ru center (see Supporting Information for electron count of **3**). Thus, clusters **2** and **3** can be considered as isoelectronic, and an interpretation of $[(Cp^*Ru)_2\{Ru(CO)_2\}_2BH(\mu_3\text{-}E)(\mu_3\text{-}H)B(\mu\text{-}H)_3\}Ru\text{-}\eta^5\text{-}\{(Cp^*Ru)_2(\mu\text{-}CO)_3(\mu\text{-}H)BH\}]$ may be used to illustrate the bonding of **3**. The calculated HOMO−LUMO gaps for compounds **2** and **3** reveal that the thermodynamic stability of **3** predominates over **2** (Table S5)

The core structure of **2** is very similar to that of **III** (Chart 1) having 60 cluster valence electrons (cves). The only difference between these two is the presence of two extra hydrogen atoms in **2** instead of a CO ligand. Therefore, DFT computations of **2** and **III** were performed to probe whether the presence of extra triply bridged hydrogens in **2** plays a significant role imparting additional stability. The results show that the thermodynamic stability of **2** is in fact more than **III** (Table S5). This stability is more likely due to the fact that there is more effective overlap for second row transition metals over those of the first row.

■ CONCLUSION

To sum up, this work describes the isolation and structural characterization of some homometallic cuboidal metallaboranes having μ_3-H as a vertex in the cubane core. Another interesting feature of these cubane clusters is the attachment of the borylene ligand to the cubane core. Investigations to evaluate the possibility of such unusual bonding situations with respect to other transition metals are underway, and we anticipate further progress in the future.

■ EXPERIMENTAL SECTION

General Procedures and Instrumentation. All syntheses were carried out under an argon atmosphere with standard Schlenk and glovebox techniques. Solvents were dried by common methods and distilled under Ar before use. Compound *nido*-**1** was prepared according to the literature method[19] while other chemicals were obtained commercially and used as received. The external reference for the ^{11}B NMR, $[Bu_4N(B_3H_8)]$, was synthesized with the literature method.[20] Thin layer chromatography was carried out on 250 mm dia aluminum supported silica gel TLC plates. NMR spectra were recorded on a 400 and 500 MHz Bruker FT-NMR spectrometer. Residual solvent protons were used as reference (δ, ppm, $CDCl_3$, 7.26), while a sealed tube containing $[Bu_4N(B_3H_8)]$ in $[d_6]$-benzene (δ_B, ppm, − 30.07) was used as an external reference for the ^{11}B NMR. Infrared spectra were recorded on a Nicolet iS10 spectrometer. Microanalyses for C and H were performed on PerkinElmer Instruments series II model 2400. Mass spectra were recorded either on Bruker Micro TOF-II mass spectrometer in ESI ionization mode or on Bruker Ultraflextreme using 2,5-dihydroxybenzoic acid as a matrix on a ground steel target plate in MALDI ionization mode.

Synthesis of 2−5. In a flame-dried Schlenk tube, *nido*-**1** (0.13 g, 0.25 mmol) and $[Ru_3(CO)_{12}]$, (1.2 g, 3.27 mmol) were thermolyzed in toluene at 90 °C for 3 h. The solvent was evaporated *in vacuo*; residue was extracted into hexane and passed through Celite. After removal of solvent the residue was subjected to chromatographic workup using silica gel TLC plates. Elution with hexane/CH_2Cl_2 (80:20 v/v) yielded orange **2** (0.05 g, 18%) and brown **3** (0.11 g, 29%). Same reaction at 60 °C for 2 h yielded yellow **4** (0.03 g, 15%), red-orange **5** (0.08 g, 35%), and trace amounts of **2** and **3**.

Data follow for **2**. ^{11}B NMR (128 MHz, $CDCl_3$, 22 °C): δ = 141.7 (br, 1B), 129.5 (br, 1B). ^{1}H NMR (400 MHz, $CDCl_3$, 22 °C): δ = 4.86 (br, 1H, BH_t), 1.95 (s, 15H, Cp*), 1.78 (s, 15H, Cp*), 1.64 (s, 15H, Cp*), −6.57 (br, 1H, Ru−H−B), −10.00 (s, 2H, Ru−H−Ru), −16.41 (s, 1H, μ_3−H). ^{13}C NMR (100 MHz, $CDCl_3$, 22 °C): δ = 195.7, 192.3 (CO), 106.8, 101.1, 99.7 (s, C_5Me_5), 11.1, 10.9, 9.5 (s, C_5Me_5). IR (hexane, cm^{-1}): 2007, 1977, 1684, 1669 (CO). Anal. Calcd (%) for $C_{36}H_{49}BO_6Ru_5$: C, 39.52; H, 4.51. Found: C, 40.25; H, 4.69.

Data follow for **3**. MS (MALDI): *m/z* 1501 $[M + H]^+$. Isotope envelope $C_{47}H_{68}B_4O_7Ru_7$ requires 1501.86. ^{11}B NMR (128 MHz, $CDCl_3$, 22 °C): δ = 151.7 (br, 1B), 128.9 (br, 2B), 95.1 (br, 1B). ^{1}H NMR (400 MHz, $CDCl_3$, 22 °C): δ = 9.84 (br, 1H, BH_t), 8.67 (br, 2H, BH_t), 1.95 (s, 15H, Cp*), 1.88 (s, 30H, Cp*), 1.76 (s, 15H, Cp*), −1.73 (br, 1H, Ru−H−B), −11.14 (br, 1H, Ru−H−B), −13.41 (s, 1H, μ_3-H), −15.72 (s, 2H, Ru−H−Ru). ^{13}C NMR (100 MHz, $CDCl_3$, 22 °C): δ = 198.1, 191.7 (CO), 103.4, 100.9, 98.4 (s, C_5Me_5), 10.7, 10.1, 9.2 (s, C_5Me_5). IR (hexane, cm^{-1}): 2470 w (BH_t) 1984, 1943, 1832, 1755 (CO). Anal. Calcd (%) for $C_{47}H_{67}B_4O_7Ru_7$: C, 37.75; H, 4.52. Found: C, 38.42; H, 4.79.

Data follow for **4**. MS (MALDI): *m/z* 779 $[M + H]^+$. Isotope envelope $C_{31}H_{52}B_3ORu_3$ requires 779.14. ^{11}B NMR (128 MHz, $CDCl_3$, 22 °C): δ = 91.4 (br, 2B), 82.3 (br, 1B). ^{1}H NMR (400 MHz, $CDCl_3$, 22 °C): δ = 5.81 (br, 1H, BH_t), 5.29 (br, 2H, BH_t), 1.81 (s, 30H, Cp*), 1.68 (s, 15H, Cp*), −14.70 (s, 1H, μ_3-H), −22.98 (s, 2H, μ_3-H). ^{13}C NMR (100 MHz, $CDCl_3$, 22 °C): δ = 194.9 (CO), 101.1, 99.3 (s, C_5Me_5), 10.6, 9.5 (s, C_5Me_5). IR (hexane, cm^{-1}): 2449 w (BH_t), 1740 (CO). Anal. Calcd (%) for $C_{31}H_{51}B_3ORu_3$: C, 47.99; H, 6.62. Found: C, 48.72; H, 6.39.

Data follow for **5**. MS (MALDI): *m/z* 726 $[M + H - 6CO]^+$. Isotope envelope $C_{21}H_{34}B_3Ru_4$ requires 726.91. ^{11}B NMR (128 MHz, $CDCl_3$, 22 °C): δ = 94.2 (br, 1B), 50.9 (br, 1B), 43.8 (br, 1B). ^{1}H NMR (400 MHz, $CDCl_3$, 22 °C): δ = 9.87 (br, 1H, BH_t), 9.54 (br, 1H, BH_t), 4.62 (br, 1H, B−H−B), 1.87 (s, 15H, Cp*), 1.81 (s, 15H, Cp*). ^{13}C NMR (100 MHz, $CDCl_3$, 22 °C): δ = 191.5, 189.8 (CO), 103.7, 101.6 (s, C_5Me_5), 10.7, 10.2 (s, C_5Me_5). IR (hexane, cm^{-1}): 2482 w (BH_t), 2040, 1974, 1948, 1711 (CO).

X-ray Structure Determination. The crystal data for **2**−**5** were collected and integrated using a Bruker AXS Kappa Apex2 CCD diffractometer, with graphite monochromated Mo Kα (λ = 0.710 73 Å) radiation at 296 K. The structures were solved by heavy atom methods using SHELXS-97 or SIR92[21a] and refined using SHELXL-97.[21b] Crystallographic data and structure refinement information for **2**−**5** are listed in Table S6.

Significant disorder was observed involving the permutation of BH and CO fragments in **2**. The structure of **2** has been refined by incorporating BH along with CO in both triply bridged sites. The disorder was suitably partitioned, and the site occupancies were refined during the initial stage of refinement. As site occupancy converges nearly 50% for each CO and BH, the same was fixed as 0.5 at final stages of refinement. The result can be interpreted as the molecule is having one triply bridged site CO and the other triply bridged site as BH for any individual molecule. In the case of compound **4**, the residual factor is on the higher side. The possible reason could be the vibrational motion of the Cp* ligands that led to the large thermal parameters of the Cp* moieties (thermal disorder). Even though the refinement program suggested splitting these atoms positions, such positions may be thermal artifacts rather than true atom position.

Computational Details. Geometry optimizations and electronic structure calculations were carried out on Gaussian09 (rev. C.01) program package[22] using BP86 functional[23] (composed of the Becke 1988 exchange functional and the Perdew 86 correlation functional) and def2-TZVP[24] basis set from EMSL Basis Set Exchange Library. The 28 core electrons of ruthenium were replaced by the quasirelativistic effective core potential def2-ECP.[25] To save computing time all the calculations were carried out with Cp (Cp = η^5-C_5H_5) model compounds instead of Cp* (Cp = η^5-C_5Me_5). The model compounds were fully optimized in gaseous state (no solvent

DOI: 10.1021/acs.inorgchem.5b01298
Inorg. Chem. 2015, 54, 8673−8678

effect) without any symmetry constraints. Frequency calculations were performed at the same level of theory to characterize the nature of the stationary point. All structures were found to be minima on the potential energy surface with real frequencies (zero negative eigenvalues of the Hessian matrices). The NMR chemical shifts were calculated on the BP86/def2-TZVP optimized geometries using the gradient corrected hybrid functional Becke−Lee−Yang−Parr (B3LYP).[26] Computation of the NMR shielding tensors employed gauge-including atomic orbitals (GIAOs).[27−29] The ^{11}B NMR chemical shifts were calculated relative to B_2H_6 (B3LYP B shielding constant 84.23 ppm) and converted to the usual [$BF_3{\cdot}OEt_2$] scale using the experimental $\delta(^{11}B)$ value of B_2H_6 16.6 ppm.[30] TMS ($SiMe_4$) was used as internal standard for the ^{1}H NMR chemical shift calculations (B3LYP H shielding constant 31.92 ppm). Population analysis was performed using natural bond orbital (NBO)[31] and Mulliken as implemented in Gaussian09. For NBO analysis, BP86 functional and 6-311g* basis set[32] (SDD-ECP[33] on Ru) were employed. Wiberg bond indices (WBIs)[34] and NBO second order perturbation energy values of some selected bonds were obtained on natural bond orbital (NBO) analysis. Calculations of absorption spectra were accomplished using time-dependent density functional theory (TD-DFT)[35] method at B3LYP/SDD-6-31g* level, and 50 monoexcitations were calculated for each species. Solvent effects were included via the polarizable continuum model (PCM).[36] The B3LYP Hamiltonian was chosen because it was proven to provide accurate structures and reasonable UV−vis spectra for a variety of chromophores[37] including organometallic complexes.[38] The assignment of the excitation energies to the experimental bands was performed on the basis of the energy values and oscillator strengths. GaussSum 3.0 was used to draw the absorption spectra.[39] The full width at half-maximum value used for the simulated spectrum was 3000 cm^{-1}. All the optimized structures and orbital graphics were generated using the Gauss view[40] and the Jmol[41] visualization programs.

■ ASSOCIATED CONTENT

Supporting Information

Supporting Information and . The Supporting Information is available free of charge on the ACS Publications website at DOI: 10.1021/acs.inorgchem.5b01298.

Figures of structures, CV details, additional data (PDF)
X-ray crystallographic file for **2**−**5** (CIF)

■ AUTHOR INFORMATION

Corresponding Author

*E-mail: sghosh@iitm.ac.in.

Notes

The authors declare no competing financial interest.

■ ACKNOWLEDGMENTS

Generous support of the Department of Science and Technology, DST (Project No. SR/S1/IC−13/2011), New Delhi, India, is gratefully acknowledged. K.Y. and D.K.R. thank the Council of Scientific and Industrial Research (CSIR). B.M. thanks IIT Madras for research fellowship. The computational facility of IIT Madras is gratefully acknowledged.

■ REFERENCES

(1) Eaton, P. E.; Cole, T. W. *J. Am. Chem. Soc.* **1964**, *86*, 3157.
(2) Stiefel, E. I.; Matsumoto. K. *Transition Metal Sulfur Chemistry*; ACS Symposium Series; American Chemical Society: Washington, DC, 1995.
(3) Fedin, V. P.; Czyzniewska, J.; Prins, R.; Weber, T. *Appl. Catal., A* **2001**, *213*, 123.
(4) *Transition Metal Sulfides: Chemistry and Catalysis*; Weber, T., Prins, R., van Santen, R. A., Eds.; Kluwer: Dordrecht, 1998.
(5) Hernandez-Molina, R.; Sykes, A. G. *Coord. Chem. Rev.* **1999**, *187*, 291.
(6) (a) Foust, A. S.; Dahl, L. F. *J. Am. Chem. Soc.* **1970**, *92*, 7337. (b) Rheingold, A. L.; Foley, M. J.; Sullivan, P. J. *J. Am. Chem. Soc.* **1982**, *104*, 4727. (c) Ciani, G.; Moret, M.; Fumagalli, A.; Martinengo, S. *J. Organomet. Chem.* **1989**, *362*, 291.
(7) (a) Merzweiler, K.; Rudolph, F.; Brands, L. *Z. Naturforsch., B: J. Chem. Sci.* **1992**, *47b*, 470. (b) Uhl, W.; Graupner, R.; Layh, M.; Schutz, U. *J. Organomet. Chem.* **1995**, *493*, C1. (c) Uhl, W.; Graupner, R.; Pohlmann, M.; Pohl, S.; Saak, W. *Chem. Ber.* **1996**, *129*, 143. (d) Power, M. B.; Barron, A. R.; Hynk, D.; Robertson, H. E.; Rankin, D. W. H. *Adv. Mater. Opt. Electron.* **1995**, *5*, 177.
(8) (a) Harlan, C. J.; Gillan, E. G.; Bott, S. G.; Barron, A. R. *Organometallics* **1996**, *15*, 5479. (b) Schulz, S.; Andruh, M.; Pape, T.; Heinze, T.; Roesky, H. W.; Haming, L.; Kuhn, A.; Herbst-Irmer, R. *Organometallics* **1994**, *13*, 4004. (c) Trinh, T.; Teo, B. K.; Ferguson, J. A.; Meyer, T. J.; Dahl, L. F. *J. Am. Chem. Soc.* **1977**, *99*, 408. (d) Simon, G. L.; Dahl, L. F. *J. Am. Chem. Soc.* **1973**, *95*, 2164. (e) Gall, R. S.; Chu, C. T.; Dahl, L. F. *J. Am. Chem. Soc.* **1974**, *96*, 4019.
(9) (a) Pipal, J. R.; Grimes, R. N. *Inorg. Chem.* **1979**, *18*, 257. (b) Bowser, J. R.; Bonny, A.; Pipal, J. R.; Grimes, R. N. *J. Am. Chem. Soc.* **1979**, *101*, 6229. (c) Thakur, A.; Sahoo, S.; Ghosh, S. *Inorg. Chem.* **2011**, *50*, 7940.
(10) (a) Geetharani, K.; Bose, S. K.; Sahoo, S.; Ghosh, S. *Angew. Chem., Int. Ed.* **2011**, *50*, 3908. (b) Lei, X.; Shang, M.; Fehlner, T. P. *Organometallics* **2000**, *19*, 4429.
(11) (a) Bose, S. K.; Geetharani, K.; Varghese, B.; Mobin, S. M.; Ghosh, S. *Chem. - Eur. J.* **2008**, *14*, 9058. (b) Bose, S. K.; Geetharani, K.; Ramkumar, V.; Mobin, S. M.; Ghosh, S. *Chem. - Eur. J.* **2009**, *15*, 13483. (c) Geetharani, K.; Bose, S. K.; Varghese, B.; Ghosh, S. *Chem. - Eur. J.* **2010**, *16*, 11357. (d) Bose, S. K.; Geetharani, K.; Ghosh, S. *Chem. Commun.* **2011**, *47*, 11996.
(12) (a) Roy, D. K.; Bose, S. K.; Anju, R. S.; Mondal, B.; Ramkumar, V.; Ghosh, S. *Angew. Chem., Int. Ed.* **2013**, *52*, 3222. (b) Geetharani, K.; Tussupbayev, S.; Borowka, J.; Holthausen, M. C.; Ghosh, S. *Chem. - Eur. J.* **2012**, *18*, 8482. (c) Ghosh, S.; Rheingold, A. L.; Fehlner, T. P. *Chem. Commun.* **2001**, 895. (d) Roy, D. K.; Bose, S. K.; Geetharani, K.; Chakrahari, K. K. V.; Mobin, S. M.; Ghosh, S. *Chem. - Eur. J.* **2012**, *18*, 9983. (e) Ghosh, S.; Lei, X.; Cahill, C. L.; Fehlner, T. P. *Angew. Chem., Int. Ed.* **2000**, *39*, 2900.
(13) (a) Ghosh, S.; Beatty, A. M.; Fehlner, T. P. *Angew. Chem., Int. Ed.* **2003**, *42*, 4678. (b) Ghosh, S.; Shang, M.; Fehlner, T. P. *J. Am. Chem. Soc.* **1999**, *121*, 7451. (c) Ghosh, S.; Fehlner, T. P.; Noll, B. C. *Chem. Commun.* **2005**, 3080. (d) Bose, S. K.; Ghosh, S.; Noll, B. C.; Halet, J.-F.; Saillard, J.-Y.; Vega, A. *Organometallics* **2007**, *26*, 5377. (e) Roy, D. K.; Bose, S. K.; Anju, R. S.; Ramkumar, V.; Ghosh, S. *Inorg. Chem.* **2012**, *51*, 10715.
(14) (a) Geetharani, K.; Bose, S. K.; Sahoo, S.; Varghese, B.; Mobin, S. M.; Ghosh, S. *Inorg. Chem.* **2011**, *50*, 5824. (b) Sahoo, S.; Reddy, K. H. K.; Dhayal, R. S.; Mobin, S. M.; Ramkumar, V.; Jemmis, E. D.; Ghosh, S. *Inorg. Chem.* **2009**, *48*, 6509. (c) Bose, S. K.; Geetharani, K.; Varghese, B.; Ghosh, S. *Inorg. Chem.* **2011**, *50*, 2445. (d) Bose, S. K.; Roy, D. K.; Shankhari, P.; Yuvaraj, K.; Mondal, B.; Sikder, A.; Ghosh, S. *Chem. - Eur. J.* **2013**, *19*, 2337.
(15) (a) Roy, D. K.; Barik, S. K.; Mondal, B.; Varghese, B.; Ghosh, S. *Inorg. Chem.* **2014**, *53*, 667. (b) Mondal, B.; Mondal, B.; Pal, K.; Varghese, B.; Ghosh, S. *Chem. Commun.* **2015**, *51*, 3828. (c) Anju, R. S.; Saha, K.; Mondal, B.; Dorcet, V.; Roisnel, T.; Halet, J.-F.; Ghosh, S. *Inorg. Chem.* **2014**, *53*, 10527.
(16) Maitlis, P. M. *Acc. Chem. Res.* **1978**, *11*, 301.
(17) Bottomley, F.; Chen, J.; MacIntosh, S. M. *Organometallics* **1991**, *10*, 906.
(18) Williams, P. D.; Curtis, M. D. *Inorg. Chem.* **1986**, *25*, 4562.
(19) Lei, X.; Shang, M.; Fehlner, T. P. *J. Am. Chem. Soc.* **1999**, *121*, 1275.
(20) Ryschkewitsch, G. E.; Nainan, K. C. *Inorg. Synth.* **1974**, *15*, 113.
(21) (a) Altornare, A.; Cascarano, G.; Giacovazzo, C.; Guagliardi, A. *J. Appl. Crystallogr.* **1993**, *26*, 343. (b) Sheldrick, G. M. *SHELXS-97*;

DOI: 10.1021/acs.inorgchem.5b01298
Inorg. Chem. 2015, 54, 8673−8678

University of Göttingen: Göttingen, Germany, 1997. (c) Sheldrick, G. M. *SHELXL-97*; University of Göttingen: Germany, 1997.

(22) Frisch, M. J.; Trucks, G. W.; Schlegel, H. B.; Scuseria, G. E.; Robb, M. A.; Cheeseman, J. R.; Scalmani, G.; Barone, V.; Mennucci, B.; Petersson, G. A.; Nakatsuji, H.; Caricato, M.; Li, X.; Hratchian, H. P.; Izmaylov, A. F.; Bloino, J.; Zheng, G.; Sonnenberg, J. L.; Hada, M.; Ehara, M.; Toyota, K.; Fukuda, R.; Hasegawa, J.; Ishida, M.; Nakajima, T.; Honda, Y.; Kitao, O.; Nakai, H.; Vreven, T.; Montgomery, J. A., Jr.; Peralta, J. E.; Ogliaro, F.; Bearpark, M.; Heyd, J. J.; Brothers, E.; Kudin, K. N.; Staroverov, V. N.; Keith, T.; Kobayashi, R.; Normand, J.; Raghavachari, K.; Rendell, A.; Burant, J. C.; Iyengar, S. S.; Tomasi, J.; Cossi, M.; Rega, N.; Millam, J. M.; Klene, M.; Knox, J. E.; Cross, J. B.; Bakken, V.; Adamo, C.; Jaramillo, J.; Gomperts, R.; Stratmann, R. E.; Yazyev, O.; Austin, A. J.; Cammi, R.; Pomelli, C.; Ochterski, J. W.; Martin, R. L.; Morokuma, K.; Zakrzewski, V. G.; Voth, G. A.; Salvador, P.; Dannenberg, J. J.; Dapprich, S.; Daniels, A. D.; Farkas, O.; Foresman, J. B.; Ortiz, J. V.; Cioslowski, J.; Fox, D. J. *Gaussian 09, Revision C.01*; Gaussian, Inc.: Wallingford, CT, 2010.

(23) (a) Schmider, H. L.; Becke, A. D. *J. Chem. Phys.* **1998**, *108*, 9624. (b) Perdew, J. P. *Phys. Rev. B: Condens. Matter Mater. Phys.* **1986**, *33*, 8822.

(24) Weigend, F.; Ahlrichs, R. *Phys. Chem. Chem. Phys.* **2005**, *7*, 3297.

(25) Andrae, D.; Haubermann, U.; Dolg, M.; Stoll, H.; Preuss, H. *Theor. Chim. Acta.* **1990**, *77*, 123.

(26) (a) Becke, A. D. *Phys. Rev. A: At., Mol., Opt. Phys.* **1988**, *38*, 3098. (b) Lee, C.; Yang, W.; Parr, R. G. *Phys. Rev. B: Condens. Matter Mater. Phys.* **1988**, *37*, 785. (c) Becke, A. D. *J. Chem. Phys.* **1993**, *98*, 5648.

(27) London, F. J. *J. Phys. Radium* **1937**, *8*, 397.

(28) Ditchfield, R. *Mol. Phys.* **1974**, *27*, 789.

(29) Wolinski, K.; Hinton, J. F.; Pulay, P. *J. Am. Chem. Soc.* **1990**, *112*, 8251.

(30) Onak, T. P.; Landesman, H. L.; Williams, R. E.; Shapiro, I. *J. Phys. Chem.* **1959**, *63*, 1533.

(31) (a) Weinhold, F. C.; Landis, R. *Valency and Bonding:A Natural Bond Orbital Donor-Acceptor Perspective*; Cambridge University Press: Cambridge, U.K, 2005. (b) Reed, A. E.; Curtiss, L. A.; Weinhold, F. *Chem. Rev.* **1988**, *88*, 899.

(32) Rassolov, V. A.; Ratner, M. A.; Pople, J. A.; Redfern, P. C.; Curtiss, L. A. *J. Comput. Chem.* **2001**, *22*, 976.

(33) Dolg, M.; Wedig, U.; Stoll, H.; Preuss, H. *J. Chem. Phys.* **1987**, *86*, 866.

(34) Wiberg, K. *Tetrahedron* **1968**, *24*, 1083.

(35) (a) Casida, M. E. *Recent Developments and Applications of Modern Density Functional Theory*; Elsevier: Amsterdam, 1996; Vol. *4*. (b) Casida, M. E.; Chong, D. P. *Recent Advances in Density Functional Methods*; World Scientific: Singapore, 1995; Vol. *1*, p 155.

(36) (a) Barone, V.; Cossi, M. *J. Phys. Chem. A* **1998**, *102*, 1995. (b) Cammi, R.; Mennucci, B.; Tomasi, J. *J. Phys. Chem. A* **1999**, *103*, 9100. (c) Klamt, A.; Schürmann, G. *J. Chem. Soc., Perkin Trans. 2* **1993**, *2*, 799. (d) Tomasi, J.; Mennucci, B.; Cammi, R. *Chem. Rev.* **2005**, *105*, 2999.

(37) For a review, see: Dreuw, A.; Head-Gordon, M. *Chem. Rev.* **2005**, *105*, 4009.

(38) Recent examples: (a) Andzelm, J.; Rawlett, A. M.; Orlicki, J. A.; Snyder, J. F. *J. Chem. Theory Comput.* **2007**, *3*, 870. (b) Nemykin, V. N.; Makarova, E. A.; Grosland, J. O.; Hadt, R. G.; Koposov, A. Y. *Inorg. Chem.* **2007**, *46*, 9591. (c) Santi, S.; Orian, L.; Donoli, A.; Durante, C.; Bisello, A.; Ganis, P.; Ceccon, A.; Crociani, L.; Benetollo, F. *Organometallics* **2007**, *26*, 5867. (d) Lage, M. L.; Fernández, I.; Mancheno, M. J.; Sierra, M. A. *Inorg. Chem.* **2008**, *47*, 5253.

(39) O'Boyle, N. M.; Tenderholt, A. L.; Langner, K. M. *J. Comput. Chem.* **2008**, *29*, 839.

(40) Dennington II., Keith, R. T.; Millam, J.; Eppinnett, K.; Hovell, W. L.; Gilliland, R. *GaussView, Version 3.09*; Semichem: Shawnee Mission, KS, 2003.

(41) *Jmol: An Open-Source Java Viewer for Chemical Structures in 3D*. http://www.jmol.org/.

DOI: 10.1021/acs.inorgchem.5b01298
Inorg. Chem. 2015, 54, 8673−8678